A Monte Carlo simulation of B-site order–disorder transformation in $Pb(Sc_{1/2}Ta_{1/2})O_3$ triggered by mechanical activation

2002 J. Phys.: Condens. Matter 14 8639

(http://iopscience.iop.org/0953-8984/14/37/301)

INSTITUTE OF PHYSICS PUBLISHING JOURNAL OF PHYSICS: CONDENSED MATTER

J. Phys.: Condens. Matter **14** (2002) 8639–8653 PII: S0953-8984(02)35124-5

A Monte Carlo simulation of B-site order–disorder transformation in $Pb(Sc_{1/2}Ta_{1/2})O_3$ triggered by mechanical activation

X S Gao[1], J Lim[1], J M Xue[1], J-S Wang[2], J-M Liu[3] and J Wang[1]

[1] Department of Materials Science, National University of Singapore, 119260, Singapore
[2] Department of Computational Science, National University of Singapore, 119260, Singapore
[3] Laboratory of Solid State Microstructures, Nanjing University, Nanjng 210093, China

E-mail: maswangj@nus.edu.sg

Received 21 March 2002
Published 5 September 2002
Online at stacks.iop.org/JPhysCM/14/8639

Abstract

Order–disorder transformation triggered by mechanical activation in a perovskite structure was observed in $Pb(Sc_{1/2}Ta_{1/2})O_3$; it is simulated using a Monte Carlo algorithm, based on the competition between mechanical activation leading to disordering and the thermal diffusion recovering the ordering. The time evolution of the long-range order (LRO) from an initial ordered state shows a steady decrease at the initial stage and then becomes more or less stabilized over a prolonged period; while from the disordered initial state, LRO increases first and then stabilizes at a similar end value. Thermal diffusion is the dominant process at relatively high temperatures, leading to the disorder-to-order transformation. The effect of mechanical activation becomes significant and results in order-to-disorder transformation at relatively low temperatures. Both the mechanical activation intensity and the vacancy migration energy exert an impact on the degree of ordering and the order–disorder transformation temperature at low temperatures. Snapshot images of the simulation demonstrate the competition between thermal diffusion and mechanical activation, which refines the domain size.

1. Introduction

Mechanical alloying has long been employed for synthesis of alloying compounds—over the past two decades [1–3]. Many interesting phenomena, such as refinement of crystallite size [4], amorphization [5], phase transitions, and chemical reactions, which may or may not be triggered by thermal activation, were observed [3, 6, 7]. Although several suggestions, such as the high pressure and high temperature at collision points [3], defect-induced amorphization [8], size-refinement-induced amorphization [3], and shearing-induced glides [9–11], have been made to account for some of these phenomena, the mechanically induced process is far from being well understood, while attempts have been made to model and simulate the process [10–17].

Mechanical activation has recently been successfully applied in the synthesis of lead-based relaxor ferroelectrics and piezoelectrics, such as $Pb(Zn_{1/3}Nb_{2/3})O_3$ [18], $Pb(Zr_xTi_{1-x})O_3$ [19], $Pb(Mg_{1/3}Nb_{2/3})O_3$ [20], and $Pb(Fe_{1/2}Nb_{1/2})O_3$ [21]. Several unique observations are associated with mechanical activation of mixed oxides, while these relaxor ferroelectrics and piezoelectrics of complex perovskite structures were formed by a single step of mechanical activation. There are also certain perovskites, which can be formed by a single step of mechanical activation, that cannot be synthesized by solid-state reaction of mixed oxides [18]. At the same time, several perovskites that can be steadily formed by solid-state reaction cannot be formed by mechanical activation [22]. Transition phases, such as the pyrochlore phases, which are always involved in the conventional solid-state reaction, are bypassed in mechanical activation [18–22]. The sequence of combining constituted oxides can have a strong effect on the thermal stability of activation-derived perovskite phases and sintering behaviours [21].

In spite of the fruitful outcomes of applying mechanical activation in synthesis of relaxor ferroelectrics, few studies have addressed the underlying phase-forming mechanisms. The physical explanations underlying many of the above phenomena remain obscure due to the complexity of the mechanical activation. We have recently observed that mechanical activation can induce order–disorder transformation in some lead-based perovskite compounds, such as $Pb(Sc_{1/2}Ta_{1/2})O_3$ and $Pb(Mg_{1/2}W_{1/2})O_3$–$Pb(Mg_{1/2}Nb_{1/2})O_3$ [23]. The order–disorder transformation is similar to that in FeAl alloys, which was demonstrated by Pochet *et al* [9], whose experimental observation and theoretical prediction suggested that such a transformation can be ascribed to the competition between thermal diffusion and mechanically induced shearing and glides [11]. Although extensive shear-induced glides may not commonly occur in bulk oxides, they have been observed in perovskite structures at elevated temperatures, and in particular in some nanocrystalline oxides, which exhibit a considerable degree of superplasticity and glide-induced behaviours [24–26]. Furthermore, the *in situ* temperature at the collision point can be very high [3].

Disordering in $Pb(Sc_{1/2}Ta_{1/2})O_3$ was previously obtained by quenching from a very high temperature (i.e., above 1500 °C) [27, 31]. We have also recently observed that mechanical activation can also trigger the B-site disordering in complex perovskite structures, such as in PMN–PMW, while the thermal activation recovers the ordering, leading us to conclude that an equilibrium state can be achieved by competition between mechanical activation and thermal diffusion [23]. B-site order–disorder transition can strongly affect the electrical and ferroelectric properties of relaxor ferroelectrics [27–31]. It is therefore both scientifically interesting and technologically challenging to investigate the order–disorder transformation in these materials.

The objectives of this work are twofold. Firstly, we examine the effects of mechanical activation on the order–disorder transformation in PST, which has long been considered as a model material for investigation of B-site ordering in complex perovskite structures [27, 31], Secondly, a Monte Carlo simulation is presented, based on the competition between the mechanical activation leading to disordering and the thermal diffusion recovering the ordering.

2. Experimental and simulation procedure

2.1. Experimental procedure

The starting materials employed in this work are commercially available PbO (99% purity, J T Baker Inc.), Sc_2O_3 (99.6% purity, J T Baker Inc.), and Ta_2O_5 (99% purity, Aldrich, USA). Single-phase PST of perovskite structure was synthesized by the columbite method: Sc_2O_3 and Ta_2O_5 were mixed and calcined at 1000 °C for 6 h forming the columbite $ScTaO_4$ phase. This

was then mixed with PbO and calcined again at 900 °C for 2 h to obtain a single perovskite phase of PST. The resulting PST was mechanically activated in a shaker-mill operated at ∼900 rpm for various time periods from 0 to 20 h to investigate the order–disorder transformation. The mechanically activated compositions were examined using x-ray diffractometry (XRD, Cu Kα), where the degree of long-range order (LRO) was calculated by comparing the peak intensity of the perovskite (200) plane and that of the superlattice (111) diffraction peak, as defined by the following equation [27, 31]:

$$\mathrm{LRO} = \left[\frac{(I_{111}/I_{200})_{observed}}{(I_{111}/I_{200})_{calculated,\ for\ S=1}} \right]^{\frac{1}{2}} \tag{1}$$

where $(I_{111}/I_{200})_{observed}$ represents the ratio between the diffraction intensities of the (111) plane and the (200) plane from XRD spectra, and $(I_{111}/I_{200})_{calculated,\ for\ S=1}$ represents the calculated value for a completely ordered material.

2.2. Modelling and simulation process

Previous studies on the B-site order–disorder transition in $A(B'B'')O_3$ complex perovskites suggest that the ordering in B sites is a result of the differences in charge and size of B-site cations [32–34]. Following these studies, we only consider the Coulomb interactions among B cations, together with the interaction of A-site cations and oxygen with B-site cations [33], and the Hamiltonian can be written as

$$\tilde{H} = \frac{e^2}{4\pi\varepsilon_0\varepsilon_r} \sum_{ij} \left(\frac{q_{i\mathrm{A}} q_{j\mathrm{B}}}{r_{ij\mathrm{AB}}} + \frac{q_{i\mathrm{O}} q_{j\mathrm{B}}}{r_{ij\mathrm{BO}}} + \frac{q_{i\mathrm{B}} q_{j\mathrm{B}}}{r_{ij\mathrm{BB}}} \right) \tag{2}$$

where ε_0 is the dielectric constant of vacuum, ε_r the relative dielectric constant, and e is the elemental electric charge unit; $q_{i\mathrm{A}}, q_{i\mathrm{O}}, q_{i\mathrm{B}}, q_{j\mathrm{B}}$ are the electric charges of A-, O-, B-site cations at the ith lattice site, and B-site cations at the jth lattice site respectively; $r_{ij\mathrm{AB}}$, $r_{ij\mathrm{BO}}$, and $r_{ij\mathrm{BB}}$ represent the distance between A and B cations, the B cation and oxygen, and B cations in the ith lattice site and the jth lattice site, respectively. In equation (2), $q_{i\mathrm{A}} = q_{\mathrm{A}}$ and $q_{i\mathrm{O}} = q_{\mathrm{O}}$ are constant in value and $q_{i\mathrm{B}}$ takes different values at the different lattice sites. Because the difference in distance between two B-site cations makes little contribution to the total energy, in comparison to those in the interaction of charges, the differences between B-site cations can be neglected [32–34]. Thus, the only variable is $q_{i\mathrm{B}}$. If $q_{i\mathrm{B}}$ is set as $q_{i\mathrm{B}} = \bar{q}_{\mathrm{B}} + \Delta q_i$, where $\bar{q}_{\mathrm{B}}$ is an average B-site charge value, which is also an invariant, Δq_i is the fluctuation of B-site charge at the ith lattice site, and its average value $\overline{\Delta q_i}$ is zero, to satisfy charge neutrality. For example, in $Pb(Sc_{1/2}Ta_{1/2})O_3$, q_{A}, q_{O}, $\bar{q}_{\mathrm{B}}$ are +2, −2, +4, respectively; and Δq_i is −1 if Sc is in the ith site, while if Ta is in the ith site Δq_i is +1. The Hamiltonian can then be written as

$$\tilde{H} = \frac{e^2}{4\pi\varepsilon_0\varepsilon_r} \sum_{ij} \frac{\Delta q_i\, \Delta q_j}{r_{ij\mathrm{AB}}} + H_0 + H_1, \tag{3}$$

where H_0 is a invariant term given by equation (4):

$$H_0 = \sum_{ij} \left(\frac{q_{\mathrm{A}} \bar{q}_{\mathrm{B}}}{r_{ij\mathrm{AB}}} + \sum_{ij} \frac{q_{\mathrm{O}} \bar{q}_{\mathrm{B}}}{r_{ij\mathrm{BO}}} \right) \tag{4}$$

and H_1 is a term linear in Δq_i, as given below:

$$H_1 = \frac{e^2}{4\pi\varepsilon_0\varepsilon_r} \left\{ \sum_i \Delta q_i \left(\sum_j \frac{q_{\mathrm{A}}}{r_{ij\mathrm{AB}}} + \sum_j \frac{q_{\mathrm{O}}}{r_{ij\mathrm{BO}}} + \sum_j \frac{\overline{q_j}}{r_{ij\mathrm{BB}}} \right) \right\}. \tag{5}$$

Because the lattice is periodic, the values of the terms inside the parentheses are independent of i; thus H_1 vanishes since $\sum_i \Delta q_i$ equals zero. For simplicity, we only consider the interactions

among nearest neighbours; equation (3) can be simplified to an Ising-type antiferromagnetic Hamiltonian, as given below:

$$\tilde{H} = J \sum_{i,j} \Delta q_i \, \Delta q_j + H_0, \tag{6}$$

where J is the constant of interaction between the B-site cations, and equals $e^2/(4\pi\varepsilon_0\varepsilon_r a_0)$, a_0 is the distance between two nearest neighbours of B-site cations, and H_0 is a constant and independent of the distribution of Δq_i.

In a three-dimensional simple cubic system, the lattice site can also be described by the lattice indices (h, m, l), where h, m, l represent the lattice indices along the a-, b-, and c-axes of the lattice cells. The lattice is also divided into two sublattices: sublattice A, where $h+m+l$ is an even number, and sublattice B, where $h+m+l$ is an odd value. Here, the LRO is defined by

$$\mathrm{LRO} = \frac{n - n_r}{n_o - n_r}, \tag{7}$$

where n, n_o, and n_r represent the number of B′ ions in A sublattices, i.e. the number of sites carrying positive Δq in sublattice A or the number of sites carrying negative Δq in sublattice B, in a partially ordered state, a completely ordered state, and a completed disordered state, respectively. If $N_{\mathrm{A}+}$, $N_{\mathrm{A}-}$, $N_{\mathrm{B}-}$, $N_{\mathrm{B}+}$ are used to represent the number of sites occupied by positive Δq in the A sublattice, negative Δq in sublattice A, negative Δq in sublattice B, and positive Δq in sublattice B, respectively, in a simple cubic lattice of size of N^3, the following equations are satisfied: $n = N_{\mathrm{A}+} = N_{\mathrm{B}-}$; $N_{\mathrm{A}-} = N_{\mathrm{B}+} = N^3/2 - N_{\mathrm{A}+}$; $n_r = N^3/4$; $n_o = N^3/2$. Therefore, one can obtain

$$\mathrm{LRO} = \frac{N_{\mathrm{A}+} - N^3/4}{N^3/4} = \frac{N_{\mathrm{A}+} - N_{\mathrm{A}-} - N_{\mathrm{B}+} + N_{\mathrm{B}-}}{N^3}. \tag{8}$$

In PST, Δq is +1 or −1, and the LRO of the charge can also be calculated from

$$\mathrm{LRO} = \frac{1}{N^3}\left|\sum_{hml} (-1)^{h+m+l} \, \Delta q_{hml}\right|. \tag{9}$$

The short-range order (SRO) is defined by [32, 35]

$$\mathrm{SRO} = \frac{nn - nn_r}{nn_o - nn_r}, \tag{10}$$

where nn_o, nn_r, nn are the number of B′–B″ pairs in a fully ordered, fully disordered, and partially ordered lattice, respectively, as given by

$$nn = \sum_{\langle ijk,hml\rangle} -(\Delta q_{ijk} \, \Delta q_{hml})_{observed}, \tag{11a}$$

$$nn_o = \sum_{\langle ijk,hml\rangle} -(\Delta q_{ijk} \, \Delta q_{hml})_{ordered}, \tag{11b}$$

$$nn_r = \sum_{\langle ijk,hml\rangle} -(\Delta q_{ijk} \, \Delta q_{hml})_{random}, \tag{11c}$$

where $\langle\,\rangle$ denotes the sum extends over the nearest neighbour (i, j, k) and (h, m, l) pairs. Thus, the SRO can also be calculated:

$$\mathrm{SRO} = \frac{\sum_{\langle ijk,hml\rangle}[(\Delta q_{ijk} \, \Delta q_{hml})_{observed} - (\Delta q_{ijk} \, \Delta q_{hml})_{random}]}{\sum_{\langle ijk,hml\rangle}[(\Delta q_{ijk} \, \Delta q_{hml})_{ordered} - (\Delta q_{ijk} \, \Delta q_{hml})_{random}]}. \tag{12}$$

Thermal diffusion of the B-site cations is achieved by the jumping of B-site vacancies, where the jumping probability of a vacancy can be written as

$$W_{if} = \nu \exp\left(-\frac{E_s}{kT}\right) \exp\left(-\frac{\Delta E_{if}}{kT}\right), \tag{13}$$

Table 1. Parameters used in the simulation in this work.

J	Δq	kT/J	γ	N	γ/N^3	E_s
1	± 1	0.5–6	10^{-5}–10^{6}	12–64	10^{10}	15–25

where ν is the atomic vibration frequency, E_s is the migration energy of the vacancy representing the energy barrier to the jumping of the vacancy, k is the Boltzmann constant, T is the temperature, and ΔE_{if} represents the difference between the B-site interaction energies before and after the jumping of the vacancy. To avoid the agglomeration effect among vacancies, only one vacancy was introduced in this system, by following the Vives and Planes method [36]. As a result, the concentration of vacancies varies with lattice size. The vacancy concentration has then to be renormalized by setting $\frac{\nu}{N^3}$ as a constant; hence a constant pre-exponential diffusion coefficient (D_0) results.

It is however difficult to give a direct comparison between what can be observed experimentally and what can be obtained by simulation. For example, the vacancy concentration, effect of plastic deformation, and migration energy of vacancies are difficult to estimate. However, the simulation can give a qualitative account of how the order–disorder transformation takes place, how the domain size changes with ordering, and the relationship between them. By setting ε_r as a constant, J becomes a constant, which is set as energy unit 1. For example, if ε_r is 100, J will be 0.034 eV. One can also set 10^9 for $\frac{\nu}{N^3}$ corresponding to a value of D_0 of $\sim 10^{-2}$ m^2 s^{-1}. The temperature used in this simulation is a normalized temperature, $\frac{kT}{J}$. The migration energy assumed in the simulation and the other parameters considered are summarized in table 1.

The intensity of the mechanical activation is described by γ, which is the ratio of the shear frequency to the atomic vibration frequency. Following Bellon and Averback [11], the time between two shear events is chosen randomly so as to reproduce an average shear frequency. Because of the periodic boundary condition, the shearing effects are introduced in pairs. One of the three $\langle 100 \rangle$ planes is randomly chosen, and the vectors of shift are also randomly selected among the four directions along the connections of nearest neighbours in the selected (100) planes. The first and last planes to be shifted are also randomly chosen. During the simulation, all the sites between the selected $\langle 100 \rangle$ planes shift, for a single lattice site, along a given direction.

In the initial stage, the system is considered as a fully ordered state, in which any two nearest neighbours carry different electrical charges, except one vacancy with zero charge. For the thermal diffusion, one of the six nearest neighbours of the vacancy is randomly chosen, and the probability of exchange between the vacancy and the selected neighbour is calculated. Following the Metropolis algorithm, the states are updated and the simulation is scaled in MC steps (mcs), while the average number of mcs between two shearing events is defined by the ratio of the jumping frequency and activation intensity, given as follows:

$$\tau = \frac{\nu}{\gamma N^3} \exp\left(-\frac{E_s}{kT}\right) \qquad \text{(in mcs)} \tag{14}$$

where γ is the frequency of the shearing events, indicating the intensity of mechanical activation. For each simulation state, the first 100 000 steps are discarded and the LRO and SRO are obtained by averaging the next 100 000–200 000 mcs.

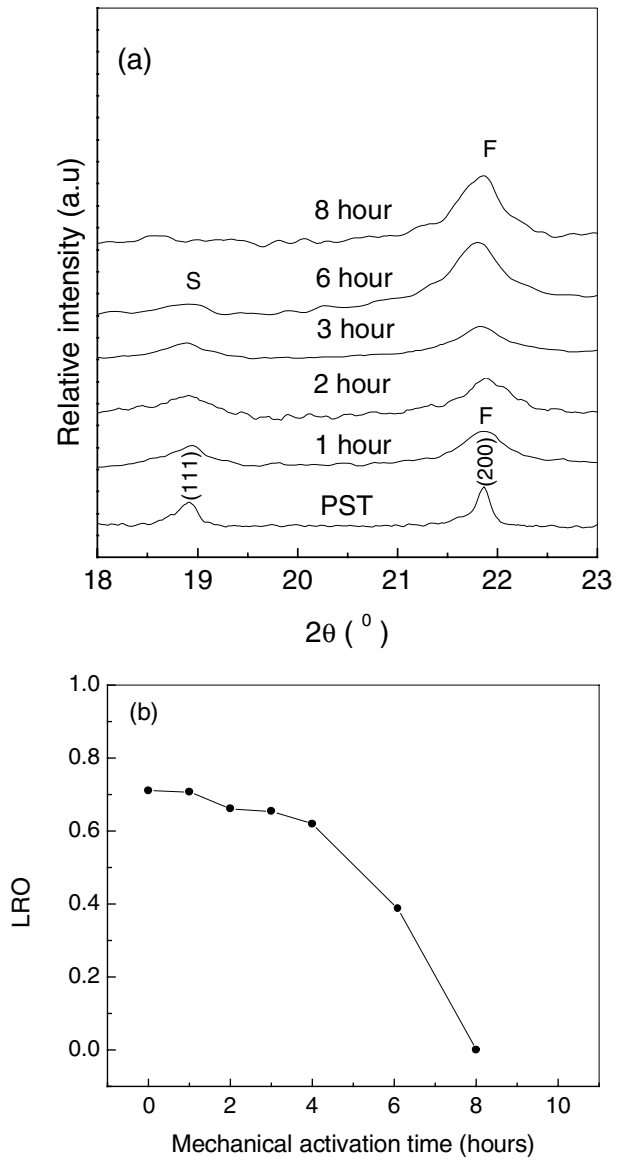

Figure 1. (a) XRD traces of PST powders subjected to various periods of mechanical activation, showing the gradual disappearance of the (111) superlattice peak. (b) The LRO as a function of mechanical activation duration. 'S': the superlattice peak; 'F': the principal diffraction peak.

3. Results and discussion

Figure 1(a) shows the θ–2θ diffraction patterns of PST samples that were subjected to various periods of mechanical activation. The unactivated PST exhibits a well-established (200) peak at around 2θ of 21.8° together with a superlattice (111) peak at 2θ of 18.9°, indicating the ordering of B-site cations [28]. Upon mechanical activation, the superlattice peak becomes broadened at the initial stage of mechanical activation, and it almost completely disappears at 8 h of mechanical activation. The crystallite size of PST calculated using Scherrer's equation

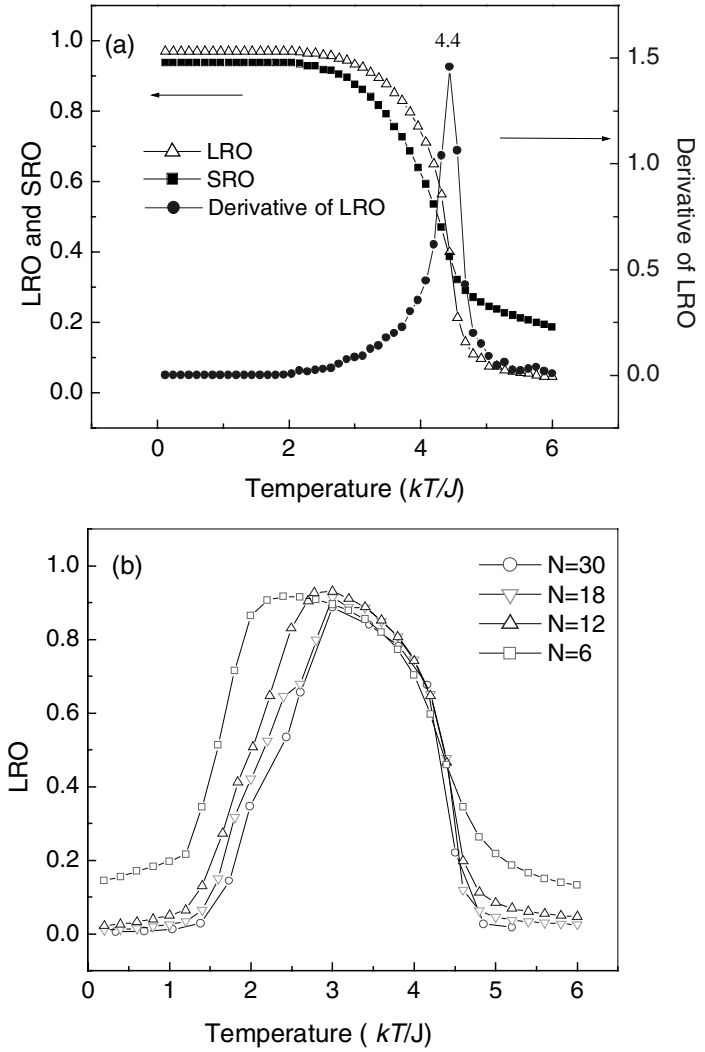

Figure 2. (a) Temperature dependences of the LRO, SRO, and derivative of the LRO, for the unactivated PST, showing an order–disorder transition at a temperature $\frac{kT}{J}$ of ∼4.4. (b) LRO as a function of temperature for mechanically activated PST at various lattice sizes. The frequency of the shearing events, γ, is 100; the vacancy migration energy, E_s, is 20.

drops dramatically from more than 1 μm to around 12 nm during the first four hours of mechanical activation [37]. The extent of LRO is calculated using equation (1) and plotted in figure 1(b) as a function of mechanical activation time. It decreases steadily in the first four hours of mechanical activation, and then falls dramatically with further duration of mechanical activation. It is almost eliminated at 8 h of mechanical activation. The mechanically induced order–disorder transformation is very similar to that in the metallic alloy FeAl, reported by Pochet *et al* [9].

The temperature dependences of the LRO and SRO of the unactivated PST from Monte Carlo simulations are shown in figure 2(a). Both the LRO and the SRO exhibit order–disorder transition at the normalized temperature of 4.4, which is defined as the maximum of the first

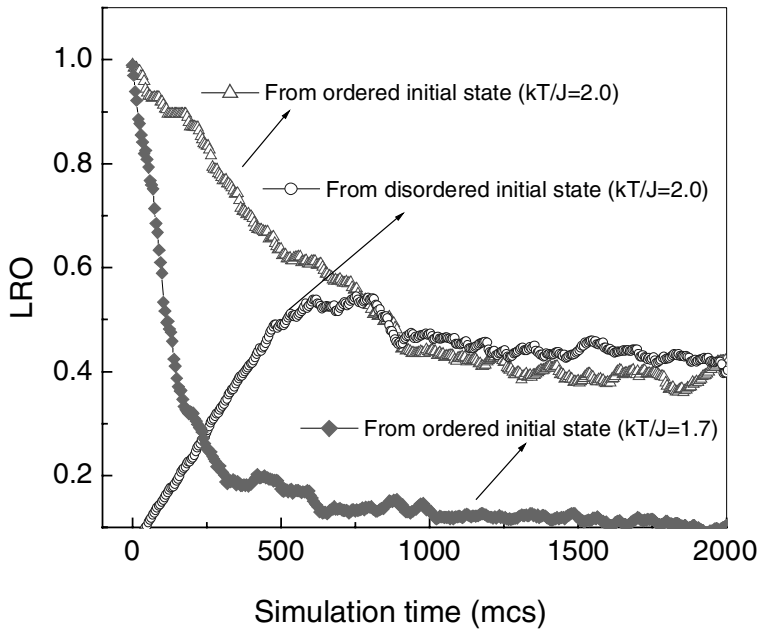

Figure 3. LRO as a function of simulation time from a full ordered initial state and a disordered initial state, respectively, at three temperatures. $\gamma = 100$; $E_s = 20$; $N = 30$. The LRO values were obtained by averaging the results of 100 simulation cycles.

derivative of the LRO. This behaviour and the transition temperature are in good agreement with the well-accepted value of the Ising-type antiferromagnetic transition point of 4.5, and the macroscopic approach of Jang *et al* [32] (transition temperature: $\frac{kT}{J} = 4.9$). Figure 2(b) shows the LRO as a function of temperature for the mechanically activated PST simulated at various lattice sizes. Similar to the case for unactivated PST, an order–disorder transition at about 4.4 is observed. With decreasing temperature, the effect of mechanical activation becomes significant, and the degree of ordering decreases with decreasing temperature depending on the lattice size, giving rise to a new order-to-disorder transformation at relatively low temperature. At the same time, the resulting LRO also changes as the lattice size (N) increases, showing some finite-size effect. When the lattice size N is large enough, the LRO is expected to be reduced at high temperatures ($\frac{kT}{J} = 3$–4.9), because a longer diffusion time is needed for a large-sized lattice to return to its thermodynamics equilibrium state within the interval of two shearing events than for a small one. However, in our experiments, it was observed that shearing during the mechanical activation refines the large crystals first, and the order–disorder transformation occurs with nanosized particles of 7–10 nm, as indicated by the XRD results. Simulation is therefore carried out using relatively small lattice sizes, giving an account for the experimentally observed phenomena.

Figure 3 shows the time evolution of the LRO for $N = 30$. At $\frac{kT}{J} = 2.0$, from an initially ordered state, the LRO decreases steadily in the first 900 mcs, and then becomes more or less stabilized; while from an initially disordered state, the LRO increases gradually at first, and is then stabilized at a similar value to that for the initially ordered state, which agrees with the statistical results of figure 2(b). At a relatively low temperature ($\frac{kT}{J} = 1.7$), the LRO drops sharply from an initially ordered state in a short period of time and gradually disappears. This is comparable to what has been observed experimentally, and is also in agreement with the

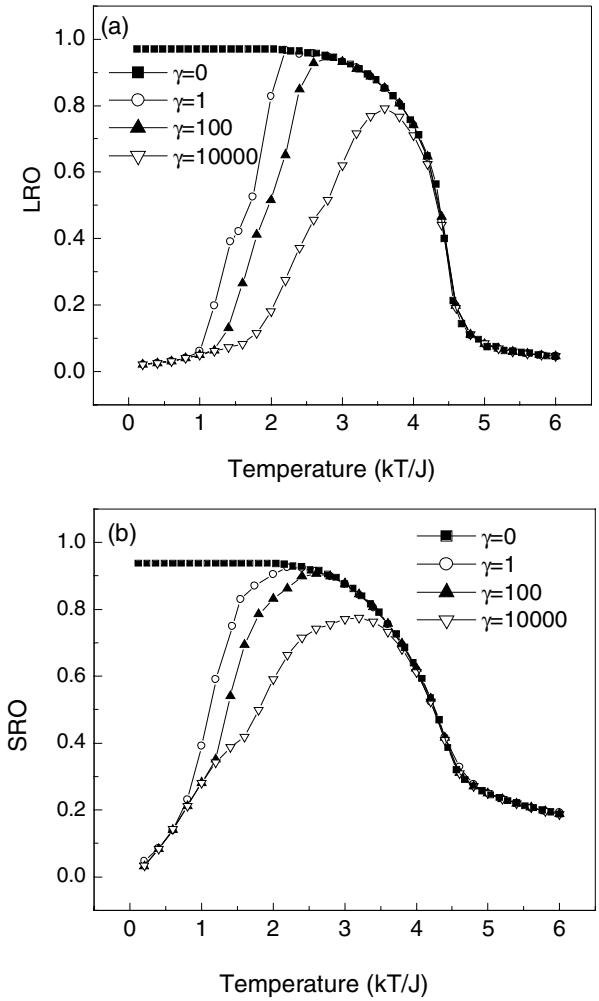

Figure 4. (a) LRO and (b) SRO, as a function of temperature, at various mechanical activation intensities. $E_s = 20$.

macroscopic approach for FeAl alloys [9]. In correlation with figure 1(b), it appears that the simulation model is more applicable to the late stage of mechanical activation (e.g. after 4 h of mechanical activation), where the crystallite size is small enough. This can be accounted for by the observation that shear-induced glides do not occur extensively in bulk oxides.

Figures 4(a) and (b) plot LRO and SRO, respectively, as a function of temperature, at various mechanical activation intensities. Increasing the mechanical activation intensity apparently has little impact on the ordering in the high-temperature order–disorder transition region; while at low temperatures, increasing activation intensity reduces the B-site ordering, and shifts the low-temperature order–disorder transformation towards a higher temperature. A similar behaviour is observed with the SRO, as shown in figure 4(b).

Figures 5(a) and (b) show the LRO and SRO, respectively, as a function of mechanical activation intensity, at three temperatures. Both the LRO and the SRO change from a fully ordered state to a highly disordered state with the increase in activation intensity. However, a higher activation intensity is required at higher temperatures for a given degree of LRO and

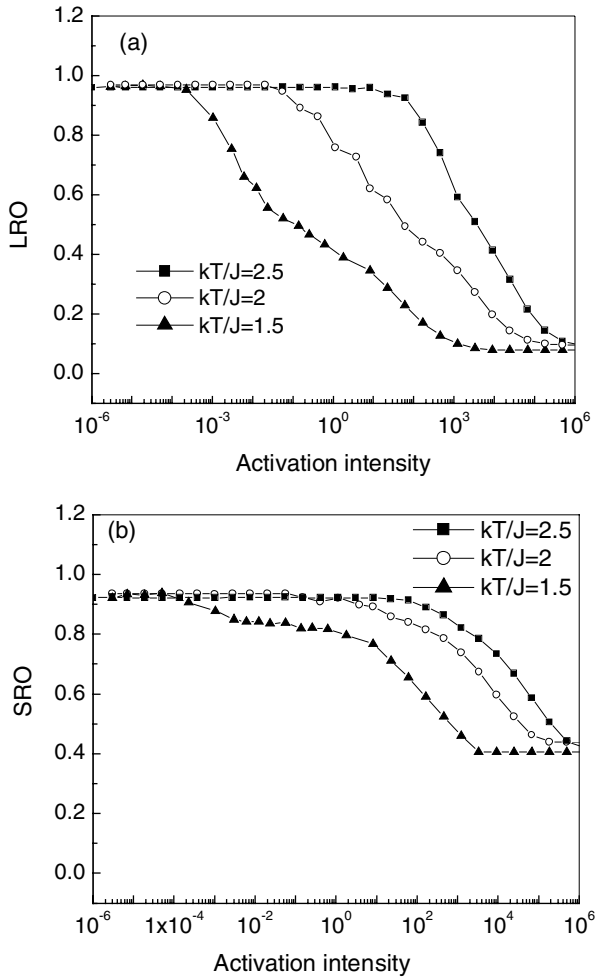

Figure 5. (a) LRO and (b) SRO, as a function of mechanical activation intensity, at various temperatures. $E_s = 20$.

SRO ordering. For example, at $\frac{kT}{J} = 1.5$, the LRO begins to fall at a mechanical activation intensity of about 2.3×10^{-4}, and approaches complete disorder at 1.2×10^{3}; while in the case of $\frac{kT}{J} = 2$, the LRO begins to drop at an intensity of 5.6×10^{-2}, and approaches the fully disorder state at 6.7×10^{4}. Similar behaviours have also been observed with the SRO. For example, significant decrease in the SRO starts at the intensity of 2.3×10^{-4} and ends approximately at 3.3×10^{3} at $\frac{kT}{J} = 1.5$; while the starting and ending intensities for $\frac{kT}{J} = 2$ are 2.2 and 1.8×10^{4}, respectively. The ending value for SRO is apparently larger than that for LRO (about 0.4), indicating the difficulty in reducing the SRO compared with the LRO. The above phenomena also suggest that a change in temperature has a significant impact on the degree of ordering during mechanical activation. This can be accounted for by two considerations. On the one hand, a low temperature reduces the migration frequency of vacancies. On the other hand, it is difficult to exchange the B-site cation with a vacancy at a low temperature. Thus, it is difficult to recover from a disordered state caused by mechanical activation at low temperatures.

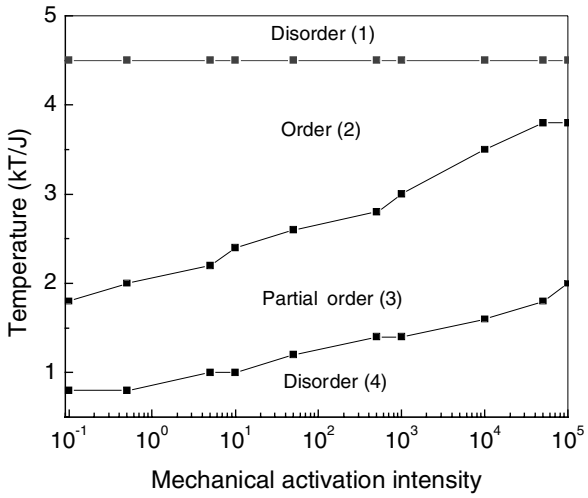

Figure 6. The phase diagram of the Monte Carlo simulation showing the different ordering states as a function of mechanical activation intensity and temperature.

On the basis of the above analyses, an order–disorder diagram of the temperature and mechanical activation intensity is constructed in figure 6. With decreasing temperature, the phase change follows the sequence: disorder to order, to partial order, and then to full disorder, corresponding to the areas marked 1 to 4 in the diagram, respectively. The transformation from area 1 to 2 is caused by the thermal diffusion, while the transformation from area 2 to 3 is a result of the competition between thermal diffusion and mechanical activation, and that from area 3 to 4 is due to the mechanical activation. With increasing mechanical activation intensity, the transformation temperature between areas 2 and 3 and that between areas 3 and 4 increase in a logarithmic manner.

A further parameter that affects the degree of ordering is the migration energy of vacancies, as shown in figure 7, by the temperature dependence of the LRO at three vacancy migration energies, 15, 20, and 25. Similar to what is shown in figure 4(a), at high temperatures (e.g. above $\frac{kT}{J} = 3$), the LRO shows, at the three vacancy migration energies, the same value as that of the unactivated PST, implying the domination of thermal diffusion at high temperatures. At low temperatures, the LRO begins to drop from the temperature of 3 and the end result is a disordered state at 1.4 for $E_s = 25$; while the starting and ending temperatures for $E_s = 15$ are 2.2 and 1.0 respectively. Since a high vacancy migration energy disfavours the migration of vacancies and slows down the thermal diffusion, the recovery of an ordered state is more difficult to realize. As a result, the degree of ordering is reduced by the mechanical activation.

To further discuss the simulation results presented above, the B-site interaction energy is calculated and is shown in figures 8(a) and (b). The interaction energy in figure 8(a), as a function of temperature at different mechanical activation intensities, demonstrates that the interaction energy of unactivated PST falls dramatically at about 4.4 (the disorder–order transition temperature), and the fall slows down with further decrease in temperature in the low-temperature region. A typical thermodynamic equilibrium behaviour is expected for the unactivated PST. When mechanical activation is applied, the interaction energy is almost the same as that of unactivated PST at high temperatures. However, there is a significant increase at low temperatures with increasing activation intensity, demonstrating a dependence on mechanical activation intensity. The minor effect of mechanical activation on interaction energy

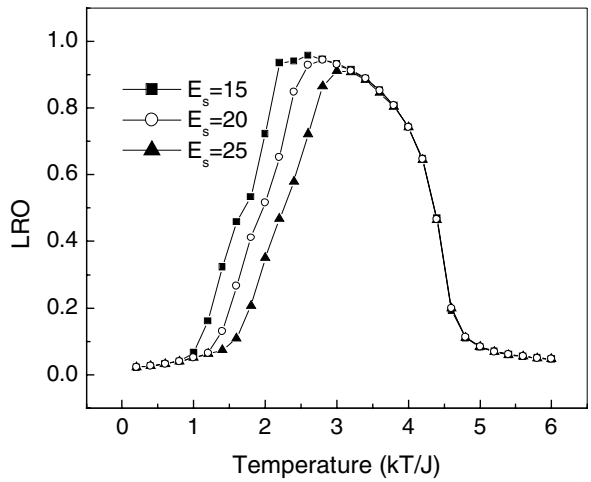

Figure 7. The simulation result for the LRO, as a function of temperature, at different vacancy migration energies.

at high temperatures can be explained by the long interval in MC steps between two shearing events as defined in equation (13) which increases dramatically with increasing temperature. For example, for a system with a shearing rate of 100 and E_s of 20, the time intervals at temperatures of 2.0, 3.0, 3.6, and 4.0 are 453, 12 726, 38 659, and 67 378 respectively. Thus, thermal diffusion is a much more significant process than the shear effect, and the system is likely to remain in a thermodynamic equilibrium state (highly ordered state). Figure 8(b) shows the temperature dependence of the interaction energy at various vacancy migration energies. Increasing migration energy enhances the interaction energy at relatively low temperatures, implying an effect of thermal diffusion. These behaviours of the interaction energy suggest that the mechanical activation is a process far from equilibrium, where the non-equilibrium state is triggered by shear effects, while the thermal activation tends to recover from a non-equilibrium state. This is also supported by the fact that a smaller interaction energy was observed for a system of lower migration energy, where the thermal diffusion becomes dominant.

To further examine the evolutions of domains upon mechanical activation, a non-equilibrium Monte Carlo simulation was carried out with a lattice size of 64^3 lattices. Although the Monte Carlo simulation may not accurately mimic the real physical evolutions, and the growth rate of domains depends on the algorithm used, one can still use the Kawasaki algorithm or vacancy diffusion algorithms to simulate the domain growth in certain systems, e.g. in the conserved order parameter (COP) Ising model system, where the simulation results fit the domain growth law very well [38, 39]. In this study, a residence-time vacancy diffusion algorithm was employed to simulate the COP Ising model, and this makes it possible to trace the evolution in physical time [40]. However, with the involvement of mechanical activation, the simulation cannot give a quantitative account of the real process, because the shear intensity and the way that shears take place cannot be accurately described. But the results presented in this study can still give a qualitative comparison between the simulation results and those for the domain evolution. Hence, the snapshot images of ordered domains in the (100) plane of a 64^3 lattice are shown in figures 9(a)–(f), which illustrates the evolution of domain disordering. A single ordered domain exists in the initial unactivated state, and it begins to split into several small ones upon mechanical activation at 20 mcs. The resulting domain boundaries are rather straight, as a result of the shearing-induced glides considered. At 100 mcs,

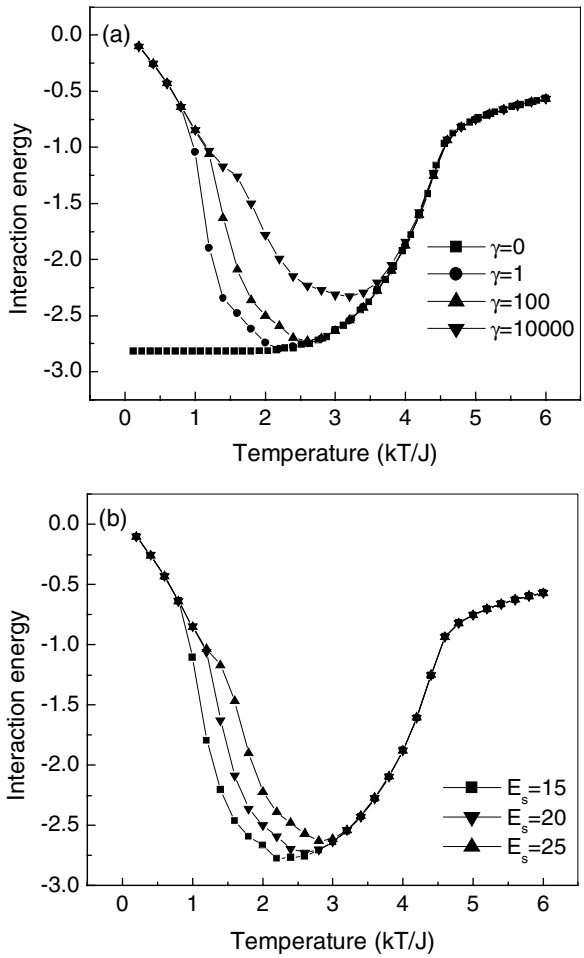

Figure 8. The B-site interaction energy as a function of temperature at: (a) various mechanical activation intensities ($E_s = 20$); and (b) various vacancy migration energies.

curved domain boundaries begin to appear, attributable to the effect of thermal diffusion, and they become apparent with increasing mechanical activation time (500 or 10 000 mcs). At 500 mcs, relatively stable domain morphology is established, although no further change can be observed with the elongated mechanical activation. A significant refinement in domain size thus takes place at the initial stage of mechanical activation, and the process slows down at 500 mcs. The building up of domain sizes by thermal activation is supported by the formation of curved domain boundaries, together with the observation that a few minor domains are trapped within big domains. It is also observed that a higher activation intensity leads to a smaller equilibrium domain size, while a higher temperature increases the domain size. The competition of mechanical activation and thermal activation then leads to a steady state in domain size with extended mechanical activation.

4. Conclusions

The order–disorder transformation in PST of perovskite structure triggered by mechanical activation has been simulated using Monte Carlo algorithm. The time evolution of LRO from

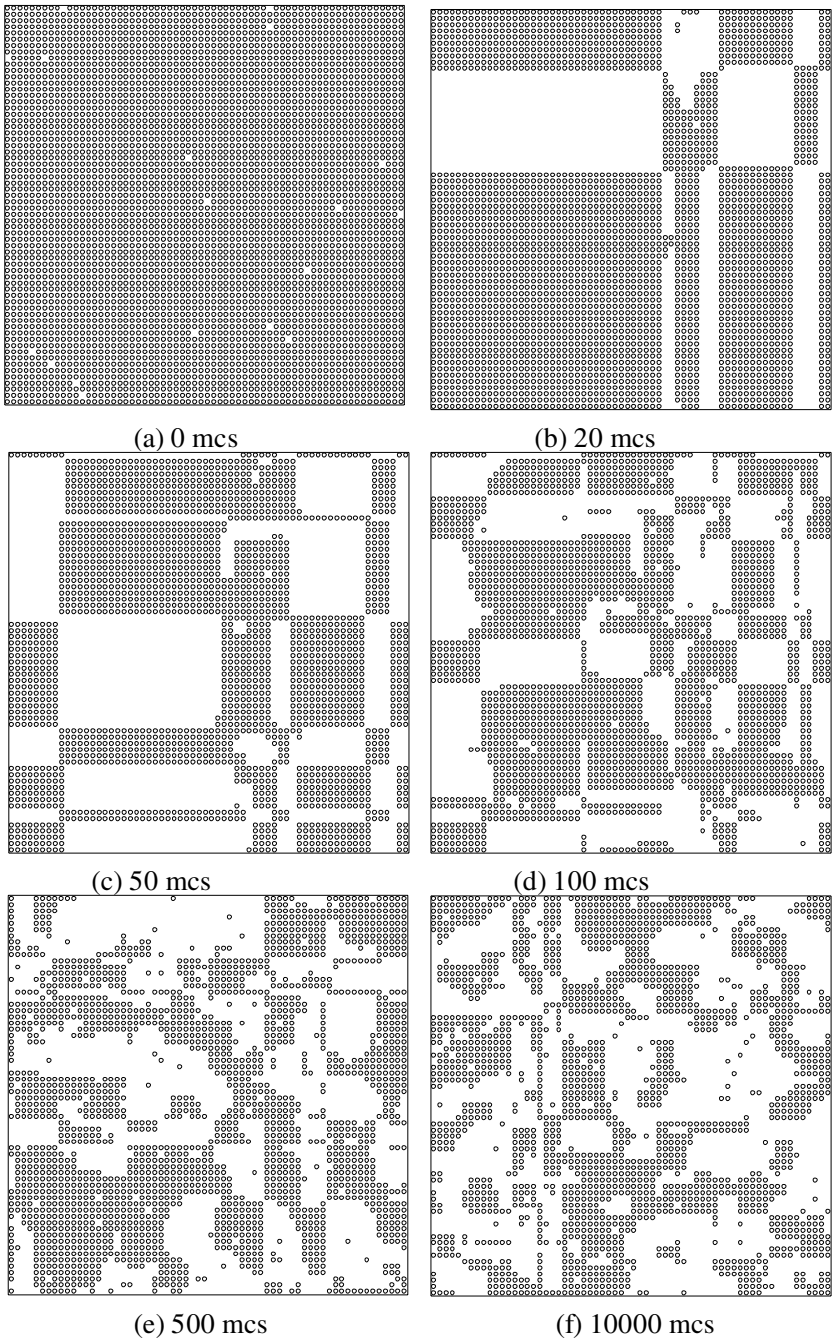

Figure 9. Snapshot images in the (100) plane of a 64^3 lattice at a temperature of 1.8, migration energy of 20, and mechanical activation intensity of 5000 upon increasing mechanical activation duration, showing the evolution of domain boundaries and domain sizes. In a given lattice site (i, j, k), if $i + j + k$ is an even number and $\Delta q = 1$ or $i + j + k$ is an odd number and $\Delta q = -1$, we have plotted an open circle; otherwise there is empty space. Thus, the areas with open circles and empty spaces indicate two different ordering domains.

the initial ordered state exhibits a steady decrease to start with, and then becomes more or less stabilized at a late stage, which is supported by experimental observation. At relatively high temperatures the transition process is controlled by thermal diffusion, while the effect of mechanical activation becomes more and more significant with decreasing temperature. Increasing the mechanical activation intensity and vacancy migration energy reduces the degree of ordering, while the low order–disorder transformation temperature is increased. The B-site interaction energy as a function of temperature shows that the mechanical activation enhances the interaction energy at around the order–disorder transformation at low temperature. The snapshot images of microscopic domains demonstrate that mechanical activation refines the domain size, while the thermal diffusion builds up domains.

References

[1] Benjamin J S 1976 *Sci. Am.* **234** 40
[2] Benjamin J S 1992 *Adv. Powder Metall. Particular Mater.* **7** 155
[3] Gaffet E, Abdellaoui M and Malhouroux-Gaffet N 1995 *Materials transaction JIM* **36** 198
[4] Sepelak V, Tkacova K, Boldyrev V V and Steinike U 1996 *Mater. Sci. Forum.* **228–231** 783
[5] Fan G J, Guo F Q, Hu Z Q, Quan M X and Lu K 1997 *Phys. Rev.* B **55** 11 010
[6] Shen T D, Koch C C, McCormick T L, Nemanich R J, Huang J Y and Huang J G 1995 *J. Mater. Res.* **10** 139
[7] Fernandez-Bertran J F 1999 *Pure Appl. Chem.* **71** 581
[8] Fecht H J 1992 *Nature* **356** 133
[9] Pochet P, Tominez E, Chaffron L and Martin G 1995 *Phys. Rev.* B **52** 4006
[10] Chen Y, Bibole M, Lehazif R and Martin G 1993 *Phys. Rev.* B **48** 14
[11] Bellon P and Averback R S 1995 *Phys. Rev. Lett.* **74** 1819
[12] Trudeau M L, Schulz R, Dussault D and Van Neste A 1990 *Phys. Rev. Lett.* **64** 100
[13] Abdellaoui M and Gaffet E 1995 *Mater. Sci. Forum.* **179–182** 339
[14] Zoltan-Juhasz A 1998 *Colloids Surf.* A **142** 449
[15] Gente C, Oehring M and Bormann R 1993 *Phys. Rev.* B **48** 13 244
[16] Yavari A R, Desre P J and Benameur T 1992 *Phys. Rev. Lett.* **14** 2235
[17] Urakaev F K and Boldyrev V V 2000 *Powder Technol.* **107** 93
[18] Wang J, Xue J M and Wan D M 2000 *Solid State Ion.* **127** 169
[19] Gan B K, Xue J M and Wan D M 1999 *Appl. Phys.* A **69** 433
[20] Xue J M, Wang J and Ng W B 1999 *J. Am. Ceram. Soc.* **82** 2282
[21] Gao X S, Xue J M and Wang J 2002 *J. Am. Ceram. Soc.* **85** 565
[22] Ang S K, Wang J and Wan D M 2000 *J. Am. Ceram. Soc.* **83** 1575
[23] Gao X S, Xue J M and Wang J 2002 *J. Am. Ceram. Soc.* **85** 833
[24] Routbort J L, Goretta K C, Cook R E and Wolfenstine 2000 *J. Solid State Ion.* **29** 53
[25] Maruyama S, Gervais A and Philibert J 1982 *J. Mater. Sci.* **17** 1384
[26] Wadsworth J and Wakai F 1991 *Int. Mater. Rev.* **36** 146
[27] Wang H C and Schulze W A 1990 *J. Am. Ceram. Soc.* **73** 1228
[28] Randall C A and Bhalla A S 1990 *Japan. J. Appl. Phys.* **29** 327
[29] Randall C A, Bhalla A S, Shrout T R and Cross L E 1990 *J. Mater. Res.* **5** 829
[30] Setter N and Cross L E 1980 *J. Mater. Sci.* **15** 2478
[31] Setter N and Cross L E 1980 *J. Appl. Phys.* **51** 4356
[32] Jang M and Kim S C 1997 *J. Mater. Res.* **12** 2118
[33] Zhang W and Wang Q 1991 *J. Am. Ceram. Soc.* **74** 2846
[34] Bellaiche L and Vanderbilt D 1998 *Phys. Rev. Lett.* **81** 1318
[35] Bethe H A 1935 *Proc. R. Soc.* A **150** 552
[36] Vives E and Planes A 1992 *Phys. Rev. Lett.* **68** 812
[37] Klug H P and Alexander L E 1954 *X-ray Diffraction Procedures for Polycrystalline and Amorphous Materials* (New York: Wiley) p 491
[38] Newman M E and Barkema G T 1999 *Monte Carlo Methods in Statistical Physics* (Oxford: Clarendon) p 269
[39] Fratzl P and Penrose O 1994 *Phys. Rev.* B **50** 3477
[40] Bortz A B, Kalos M H and Lebowitz J L 1975 *J. Comput. Phys.* **17** 10